

# ZeroVL: A Strong Baseline for Aligning Vision-Language Representations with Limited Resources

Quan Cui<sup>1,2</sup> Boyan Zhou<sup>1</sup> Yu Guo<sup>1,3</sup> Weidong Yin<sup>1</sup> Hao Wu<sup>1\*</sup> Osamu Yoshie<sup>2</sup>

<sup>1</sup>ByteDance <sup>2</sup>Waseda University <sup>3</sup>Fudan University

cui-quan@toki.waseda.jp, yuguo19@fudan.edu.cn,

{zhouboyan, yinweidong, wuhao.5688}@bytedance.com, yoshie@waseda.jp

## Abstract

Pioneering dual-encoder pre-training works (e.g., CLIP and ALIGN) have revealed the potential of aligning multi-modal representations with contrastive learning. However, these works require a tremendous amount of data and computational resources (e.g., billion-level web data and hundreds of GPUs), which prevent researchers with limited resources from reproduction and further exploration. To this end, we explore a stack of simple but effective heuristics, and provide a comprehensive training guidance, which allows us to conduct dual-encoder multi-modal representation alignment with limited resources. We provide a reproducible strong baseline of competitive results, namely ZeroVL, with only 14M publicly accessible academic datasets and 8 V100 GPUs. Additionally, we collect 100M web data for pre-training, and achieve comparable or superior results than state-of-the-art methods, further proving the effectiveness of our method on large-scale data. We hope that this work will provide useful data points and experience for future research in multi-modal pre-training. Our code is available at <https://github.com/zerovl/ZeroVL>.

## 1. Introduction

Large-scale representation pre-training has become the de-facto approach in vision [6, 7, 18, 51], language [11, 20, 32] and vision-language [23, 38] modeling tasks. In the vision-language pre-training field, most mainstream approaches fall into one of two classes: single-encoder [8, 14, 21, 24, 30, 31, 41, 44, 56] and dual-encoder [23, 35, 38, 45]. Typical single-encoder approaches focus on learning semantic alignments between image regions and text entities with a single backbone network, greatly benefiting various downstream multi-modal tasks, e.g., VQA [1, 16, 55], VCR [53] and NLVR [42, 43], etc. In real-scenario applications [37],

method	computation		data	MSCOCO		F30K	
	device	count		zs.	ft.	zs.	ft.
CLIP [38]	V100	256	400M	400.2	–	540.6	–
ALIGN [23]	TPU <sub>v3</sub>	1,024	1800M	425.3	500.4	<b>553.3</b>	<b>576.0</b>
baseline	V100	8	14.2M	363.5	471.9	476.8	553.0
ZeroVL	V100	8	14.2M	425.0	485.0	536.2	561.6
ZeroVL†	V100	8	100M	<b>442.1</b>	<b>500.5</b>	546.5	573.6

Table 1. Statistics of training resources and cross-modal retrieval RSUM scores [4, 5, 49]. “zs.” and “ft.” represent zero-shot and fine-tuned settings. “†” means pre-training with 100M web data.

dual-encoder pre-training approach could be preferable for its flexibility. For one thing, downstream tasks of either modality can benefit from the pre-training. For another, dual-encoder approaches are more efficient than single-encoder approaches on popular multi-modal industrial applications, e.g., cross-modal matching and retrieval tasks [5, 22].

Recent works [23, 38] demonstrated that, by aligning visual and language representations with the contrastive loss, a simple dual-encoder architecture is able to yield state-of-the-art representation learning performances. However, we notice two significant problems which might obstruct the progress in this research direction. (1) Pioneering works require a tremendous amount of vision-linguistic corpus and computational resources for training, and (2) there is no benchmark with only publicly accessible academic datasets for ensuring the reproduction of results. CLIP [38] and ALIGN [23] respectively collected 400M and 1.8B web image-text pairs and trained models with 256 V100 GPUs and 1,024 TPU cores. Such experimental environments challenge reproductions and further explorations for researchers with limited computation and data resources. It further leads to a lack of commonly acknowledged benchmarks, making it hard to validate the effectiveness of novel methods.

To alleviate the problems above, we provide a comprehensive training pipeline with only open-source academic datasets and limited computational resources. For reproducibility, we firstly leverage academic datasets to create a naive baseline. Then, we explore a collection of simple but

\* Corresponding author

effective heuristics, including original and existing ones, to boost model performances while only introducing marginal overhead to both computation and implementation. Many of these heuristics are inconspicuous but contribute to surprising improvements. Finally, as shown in Table 1, we stack the collection of simple heuristics and achieve competitive results with  $\sim 14\text{M}$  academic data and 8 V100 GPUs. To further demonstrate the effectiveness of our method on large-scale data, we collect 100M web image-text images and conduct pre-training without fine-tuning hyper-parameters. Surprisingly, our method successfully outperforms CLIP and achieves comparable results with ALIGN on pre-training and fine-tuning tasks.

**Contributions.** We explore a stack of simple but effective heuristics for dual-encoder vision-language representation pre-training, including originally proposed and existing ones, and offer a reproducible strong baseline for the first time in this field. More importantly, we present a resource-friendly solution for studying this topic and achieve competitive model performance. We also demonstrate the effectiveness of our method on large-scale data.

## 2. Related Works

Mainstream multi-modal pre-training methods are divided into two classes: single-encoder and dual-encoder.

*Single-encoder methods* [8, 14, 21, 24, 29–31, 41, 44, 56] typically map image and text representations with a shared encoder, *e.g.*, BERT [11]. However, jointly mapping representations from multiple modals exponentially increases the computation complexity, and these methods could be impractical for industrial cross-modal retrieval tasks [5].

*Dual-encoder methods* [23, 35, 38, 45] are flexible and inherently suitable for cross-modal retrieval tasks. This paper closely relates to dual-encoder methods CLIP [38] and ALIGN [23], which have demonstrated the potential of aligning multi-modal representations with the contrastive loss. Although great improvements have been made, these works require a tremendous amount of data and computational resources, *e.g.*, billion-level web data and hundreds of GPUs. Such experimental environments will challenge reproductions and further explorations for researchers with limited data or computational resources. This paper aims to address this problem by providing a training guideline and a reproducible strong baseline with limited resources.

## 3. A Naive Baseline

In this section, we build up a naive baseline for stacking our heuristics and polishing it to a strong one. Heuristics are divided into *data preparation*, *model architecture*, and *training* aspects, which will be discussed in Sec. 4, 5 and 6.

	Pre-training					Test	
	Total	SBU	VG	CC3M	CC12M	MSCOCO	F30K
#image	14.23M	0.86M	0.50M	2.81M	10.06M	5K	1K
#text	14.23M	0.86M	0.50M	2.81M	10.06M	25K	5K

Table 2. The statistics of datasets for pre-training and test.

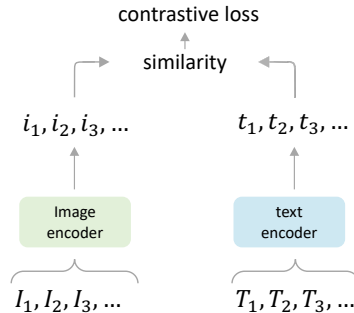


Figure 1. Illustration of the dual-encoder model architecture.

### 3.1. Pre-Training Datasets

To ensure reproducibility, only publicly accessible academic datasets are leveraged to demonstrate the effectiveness of our heuristics. The statistics of collected image-text pair datasets are reported in Table 2. Four widely-used image-text pair datasets are selected for pre-training, *i.e.*, (1) *SBU Captioned Photos (SBU)* [36], (2) *Visual Genome (VG)* [28], (3) *Conceptual Captions 3M (CC3M)* [40], and (4) *Conceptual 12M (CC12M)* [3] datasets. Due to the page limit, detailed introductions are attached in the appendix.

### 3.2. Baseline Settings

Baseline settings are elaborated from the following three perspectives, from which our heuristics derive.

**Data preparation.** Batches are comprised by randomly sampling image-text pairs from pre-training datasets. Following [23, 38], each image is randomly cropped to a rectangular region with aspect ratio sampled in  $[3/4, 4/3]$  and area sampled in  $[60\%, 100\%]$ , then resized to  $224 \times 224$  resolution. Regarding the corresponding text, we use a percentage of 20% input words for processing. For each word, we mask it, replace it with a random word, or delete it with a probability of 50%, 10% and 40%, respectively. During test, images are resized to  $256 \times 256$  and center cropped to  $224 \times 224$ , while no specific process is applied to texts.

**Model architecture.** Inspired by [23, 38], we employ a simple dual-encoder model to align visual and language representations of image-text pairs via a contrastive loss. The framework is illustrated in Figure 1. Image and text encoders are ViT-B/16 [12] and BERT-Base [11], respectively. The image encoder is pre-trained on ImageNet-21K [10] while the text encoder is pre-trained on BookCorpus [26] and English Wikipedia. [CLS] tokens from image and text encoders are extracted and then projected to compact embeddings for calculating the contrastive loss.

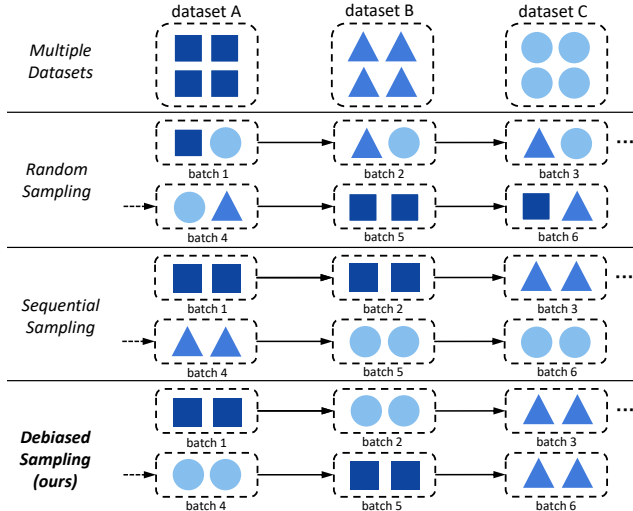


Figure 2. Illustration of sampling strategies.

**Training.** AdamW [25,34] optimizer is used for training and the weight decay is  $1e-3$ . The dual-encoder model is trained for 20 epochs on 8 Nvidia V100 GPUs with a batch size of 1,024. The learning rate is initialized to  $1e-4$  and follows a cosine decay schedule. Notably, we set a minimum learning rate  $1e-5$  to avoid over-fitting. The embedding dimension for image and text representations is 512 and the trainable temperature of contrastive loss is initialized to 0.02.

### 3.3. Evaluations

**Metrics.** Typically, multi-modal retrieval tasks are assessed with the recall at K (R@K) metric, with  $K = \{1, 5, 10\}$ . We follow [4, 5, 49] to use RSUM as the metric to reveal the overall performance of models, which is defined as the sum of recall metrics at  $K = \{1, 5, 10\}$  of both image-to-text and text-to-image retrieval tasks.

**Test datasets.** Following the standard practice in [4, 5, 13, 23, 38, 49], we evaluate representations of pre-trained models by carrying out *zero-shot* image-text retrieval tasks on test sets of (1) *MS-COCO Captions Karpathy’s split (MSCOCO)* and (2) *Flickr 30K (F30K)* datasets. MSCOCO and F30K results are reported with 5K and 1K test images, respectively.

## 4. Data Preparation

To construct vision-linguistic corpus, the common practice is to collect datasets from multiple sources. Due to the copyright or technical issues, publicly accessible image-text academic datasets are greatly limited. In this section, we study how to take full advantages of limited academic data from two perspectives, *i.e.*, (1) handling multi-source data and (2) creating extra data with augmentation.

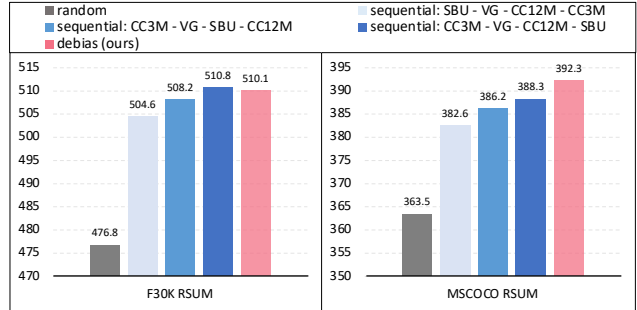


Figure 3. Comparisons between random and sequential sampling.

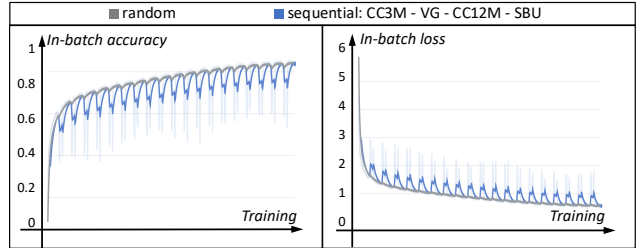


Figure 4. In-batch statistics of random and sequential sampling.

### 4.1. Handling the Multi-Source Data

**Random sampling vs. sequential sampling.** Instinctively, there are two strategies to sample training batches from multiple datasets, *i.e.*, random sampling and sequential sampling. Random sampling is a widely used method, which randomly constructs training batches with all available data. Sequential sampling, as the name suggests, pre-defines the sampling order of multiple datasets and generates batches from the sequence of datasets. Illustrations of both sampling strategies are shown in Figure 2 and experimental results are reported in Figure 3. Surprisingly, we notice the following phenomena on down-stream tasks: (1) Sequential sampling yields significantly better results than random sampling. (2) The order of datasets in sequential sampling exerts non-negligible influences on final performances. In the following, we further discuss these observations.

(1) *What makes random sampling worse?* Since the dual-encoder model is optimized by contrastive loss (*i.e.*, InfoNCE loss), we simply visualize the training accuracy within each batch in Figure 4. Consistently, the in-batch accuracy of random sampling is greater than that of sequential sampling, reflecting that models are prone to over-fit training data with random sampling. More concretely, when a batch is composed of samples from different datasets, models could be driven to distinguish negative samples by hacking the source information, *i.e.*, learning the dataset bias. For instance, dataset A is mainly composed of *natural scenery photos with long captions*, while dataset B is mainly comprised of *people with short captions*. To distinguish samples from A and B, models are allowed to remember the dataset

bias on image contents and caption lengths. However, knowledge of the dataset bias is not beneficial for downstream tasks and can be even harmful for learning essential semantic concepts, resulting in unsatisfactory generalizability.

(2) *Why does the order matter?* It is observed that adjusting the order of datasets in sequential sampling exerts non-negligible influences on model performances. We conjecture that the domain relevance between the “last seen” dataset and the downstream dataset is directly proportional to model performances, especially for zero-shot scenarios. For instance, SBU, MSCOCO, and F30K provide images with visually relevant captions, while CC3M and CC12M contain images coupled with noisy or visually irrelevant captions. Results in Figure 3 validate that setting SBU as the last dataset leads to consistently superior results, compared with CC3M or CC12M being the last one.

**Debiased sampling.** For sequential sampling, undoubtedly, enumerating the order of collected datasets is not acceptable for real-scenario applications, and the sequence needs further adjustment if new datasets are introduced. For random sampling, there is no sequence to consider, but the dataset bias problem leads to unsatisfactory performances. To tackle these problems, the key factor is forcing the model to focus on helpful knowledge instead of the dataset bias. Inspired by this, we propose the debiased sampling strategy. As illustrated in Figure 2, debiased sampling ensures instances within each batch come from the same dataset, while the order of sampled datasets is random. For example, the first batch consists of samples from only SBU, and the second batch is composed of samples of only CC3M. Under this regularization, models are not allowed to hack the optimization by remembering the dataset bias. Besides, it tackles the problem of enumerating the order of datasets in sequential sampling. As shown in Figure 3, our debiased sampling can achieve comparable performances to the specifically designed sequential sampling strategy.

## 4.2. Data Augmentation

Intuitively, data augmentation is a ubiquitous method to create extra training data. With limited data resources, the augmentation plays an important rule in boosting performances. This part will discuss two data augmentation heuristics, which bring in little computational complexity but remarkably improve model performance.

**AutoAugment.** Popular data augmentation strategies on the image modal are manually designed and mainly focus on cropping, flipping and resizing operations. Recently, the AutoAugment technique [9] has been proposed to search data augmentation policies with Reinforcement Learning automatically. Unlike cropping or resizing strategies, AutoAugment considers a wide range of operations, including translation, rotation, and color normalization. Since Au-

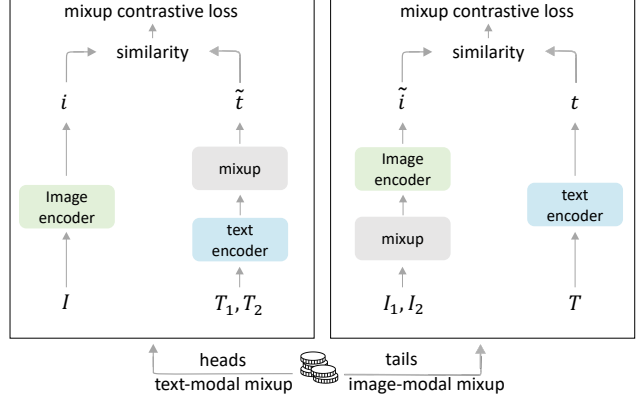


Figure 5. Illustration of our proposed coin flipping mixup. Note that manifold mixup is applied on the text modality, since we empirically observe that interpolating sparse word embeddings could lead to significant performance drop.

toAugment has shown great potential in diverse computer vision tasks, we directly apply the strategy searched on ImageNet [10] to create extra training images.

**Coin flipping mixup.** To the best of our knowledge, mixup techniques [17, 48, 52, 54] are seldom investigated in the vision-language pre-training task. In this part, we first formulate the common mixup strategy in the dual-encoder training scheme, and reveal the label assignment dilemma when calculating contrastive loss. To solve this dilemma, we further propose a novel mixup strategy named coin flipping mixup. (1) *Formulation.* We follow the previous works [17, 54] by applying instance-level mixup. Given a batch of N image-text pairs, the image and text of the  $j$ -th pair are denoted by  $I_j$  and  $T_j$ , respectively. Instead of randomly mixing image-text pairs within the batch, we leverage a more efficient mixing operation for easy implementations:

$$\begin{aligned}\tilde{I}_j &= \lambda * I_j + (1 - \lambda) * I_{N-j}, \\ \tilde{T}_j &= \lambda * T_j + (1 - \lambda) * T_{N-j},\end{aligned}\tag{1}$$

where  $\tilde{I}_j$  and  $\tilde{T}_j$  denote the  $j$ -th mixed image and text.  $\lambda$  is sampled from the distribution  $Beta(\alpha, \alpha)$ . Therefore, the training batch after the mixing operation could be denoted by  $\{(\tilde{I}_1, \tilde{T}_1), (\tilde{I}_2, \tilde{T}_2), \dots, (\tilde{I}_N, \tilde{T}_N)\}$ . However, we will encounter a label assignment dilemma. For instance, both  $(\tilde{I}_j, \tilde{T}_j)$  and  $(\tilde{I}_{N-j}, \tilde{T}_{N-j})$  are contained in the batch but interpolated by the same instances. It is not feasible to measure the target matching score between  $\tilde{I}_j$  and  $\tilde{T}_{N-j}$ . Particularly, the  $\tilde{I}_j$  and  $\tilde{T}_{N-j}$  are written as:

$$\begin{aligned}\tilde{I}_j &= \lambda * I_j + (1 - \lambda) * I_{N-j}, \\ \tilde{T}_{N-j} &= (1 - \lambda) * T_j + \lambda * T_{N-j},\end{aligned}\tag{2}$$

where the similarity between  $\lambda * I_j$  and  $(1 - \lambda) * T_j$  is not measurable based on the prior knowledge of mixup [54].

(2) *Coin flipping mixup.* To tackle the above problem, we propose the coin flipping mixup strategy. Briefly, mixup

	MSCOCO (5K test set)							Flickr30K (1K test set)						
	image → text			text → image				RSUM	image → text			text → image		
	R@1	R@5	R@10	R@1	R@5	R@10			R@1	R@5	R@10	R@1	R@5	R@10
baseline	45.1	71.5	81.6	33.9	60.3	71.1	363.5	66.0	88.9	94.1	56.2	82.4	89.2	476.8
+ debiased sampling	53.2	78.2	86.4	36.7	63.7	74.1	392.3	78.8	94.5	98.2	61.2	86.3	91.9	510.1
+ autoAugment	52.5	78.7	86.5	37.8	64.8	75.1	395.5	79.6	95.0	97.2	61.6	86.5	92.4	512.3
+ coin flipping mixup	53.0	79.8	87.6	39.6	66.2	76.5	402.8	80.1	95.7	98.4	63.7	88.2	93.1	519.2

Table 3. Results of stacking data preparation heuristics.

is applied on *one of the multiple modals* in each training batch, avoiding the above label assignment dilemma. In our implementation, by uniformly sampling  $\gamma$  from the range  $[0, 1]$ , we enable the mixup on image modal if  $\gamma > 0.5$ , otherwise text modal. Interestingly, as shown in Figure 5, the strategy is similar to the coin flipping decision-making procedure, from which its name derives.

We briefly formulate the learning objective of coin flipping mixup, assuming  $\gamma > 0.5$  and the mixup on image modal is enabled. In literature [23, 38], the contrastive loss could be disentangled to image-to-text and text-to-image matching parts. Correspondingly, the mixup contrastive loss of image-to-text matching is written as:

$$\begin{aligned} \mathcal{L}_{\tilde{I}2T} = & \lambda * \left( -\frac{1}{N} \sum_{j=1}^N \log \frac{\exp(\tilde{i}_j \cdot t_j / \tau)}{\sum_{k=1}^N \exp(\tilde{i}_j \cdot t_k / \tau)} \right) \\ & + (1 - \lambda) * \left( -\frac{1}{N} \sum_{j=1}^N \log \frac{\exp(\tilde{i}_j \cdot t_{N-j} / \tau)}{\sum_{k=0}^{N-1} \exp(\tilde{i}_j \cdot t_{N-k} / \tau)} \right), \end{aligned} \quad (3)$$

where  $\tilde{i}_j$  and  $t_j$  respectively denote representations of the mixed image  $\tilde{I}_j$  and the non-mixed text  $T_j$ . The text-to-image matching part shares similar formulations.

### 4.3. Experiment Results

Main results of data preparation heuristics are reported in Table 3. Overall speaking, all data preparation heuristics benefit performances on both F30K and MSCOCO. Note that these experiments only involve 14M academic data. Stacking these heuristics jointly contributes to +42.4 and +39.3 RSUM improvements on F30K and MSCOCO, respectively. Undoubtedly, properly leveraging limited data is of vital importance, and our heuristics are beneficial.

**Effect of debiased sampling.** Compared to the baseline, debiased sampling achieves consistent and remarkable improvements on all metrics, without any extra computational costs and hyper-parameters. Additionally, we compare the debiased sampling with other sampling methods. As aforementioned in Figure 3, the result of debiased sampling and the best result of sequential sampling are comparable, even the order of datasets is carefully adjusted. It further validates the effectiveness of our proposed debiased sampling.

**Effect of AutoAugment.** Suggested by the results, AutoAugment also introduces satisfactory improvements, bringing in minor CPU computation overhead in the data aug-

mentation process. It improves the RSUM of F30K and MSCOCO by +2.2 and +3.2, respectively.

**Effect of coin flipping mixup.** We set the alpha value of the beta distribution to 0.1, then apply input mixup on image modal and manifold mixup on text modal. Noticeable promotions are contributed by the coin flipping mixup, especially on text-to-image (T2I) metrics, *i.e.*, T2I R@1 on F30K and MSCOCO are improved by +2.1 and +1.8.

## 5. Model Architecture

We notice that previous works uses extremely large models and input resolutions for better performances, *e.g.*, EfficientNet L2 with  $289 \times 289$  resolutions [23, 46, 50] and ViT-L/14 with  $336 \times 336$  resolutions [12, 38]. Such models are not friendly to researchers with limited computational resources. To this end, we investigate how to choose efficient but powerful encoders.

Due to the success of BERT models [11, 20, 32] in natural language modeling tasks, the choice of text encoder backbone leaves us little space to explore. However, the superior architecture of the image encoder backbone remains uncertain. To this end, we focus on the selection of image encoders by finding an optimal trade-off between model performance and training efficiency.

### 5.1. CNN vs. ViT

Convolutional neural networks (CNNs) and vision transformers (ViTs) are representative image encoders. CNN is typically stacked by residual convolution blocks while ViT is mainly composed of multi-head attention blocks. Recent works [12, 33] have demonstrated the great potential of pre-trained ViTs on computer vision tasks. Additionally, since the ViT shares similar basic blocks with the BERT, employing ViT as image encoders could be helpful for capturing the correlation between image patches and key text entities.

**Model performance.** In previous works [23, 38], CNNs and ViTs achieved comparable performances on both pre-training and transferring phases. Yet, such comparisons are not under the same training setting, *e.g.*, different training resolutions and model capacities. In this part, we select comparable models and empirically compare performances between CNNs and ViTs. For reducing the uncertainty of experiment results, we train all considered models with identical hyper-parameters and pre-training datasets, without

	#params (M)	GPU time (hr)	MSCOCO (5K test set)							Flickr30K (1K test set)						
			image → text			text → image				image → text			text → image			
<i>CNN</i>			R@1	R@5	R@10	R@1	R@5	R@10	RSUM	R@1	R@5	R@10	R@1	R@5	R@10	RSUM
ResNet50×3	217	~1470	38.5	65.8	76.4	30.5	57.3	68.1	336.6	57.4	86.9	93.2	54.0	81.2	88.5	461.2
EfficientNetV2-L	120	~1480	41.8	68.6	79.4	32.3	59.0	69.9	351.1	60.4	84.3	92.7	55.3	81.7	88.7	463.0
<i>ViT</i>			R@1	R@5	R@10	R@1	R@5	R@10	RSUM	R@1	R@5	R@10	R@1	R@5	R@10	RSUM
ViT-B/16	87	~430	45.1	71.5	81.6	33.9	60.3	71.1	363.5	<b>66.0</b>	88.9	94.1	56.2	82.4	89.2	476.8
SwinT-B	87	~580	<b>46.3</b>	<b>72.6</b>	<b>81.9</b>	<b>35.7</b>	<b>62.3</b>	<b>72.9</b>	<b>371.6</b>	65.9	<b>89.7</b>	<b>95.4</b>	<b>59.7</b>	<b>85.3</b>	<b>91.2</b>	<b>487.2</b>

Table 4. Performances of various image encoders.

the aforementioned data preparation heuristics. For CNNs, ResNet50x3 [19, 27] and EfficientNetV2-L [47] are selected. Regarding ViTs, we choose ViT-B/16 [12] and SwinT-B [33]. As reported in Table 4, with the same input size (224×224 resolutions) and less model parameters, ViTs outperforms CNNs by large margins.

**Training efficiency.** To further compare the training efficiency of these encoders, we measure the training computational costs by reporting GPU time in Table 4. For training ViT-B/16, around 430 V100 GPU hours are required. For training EfficientNetV2-L and ResNet50×3, ~1500 V100 GPU hours are required. Obviously, CNNs require longer training time or more GPUs than ViTs, *e.g.*, EfficientNetV2-L almost quadruple the training time of ViT-16/B, but higher performances are achieved by ViTs, further validating its superiority. Additionally, SwinT-B costs around 30% longer training time than ViT-16/B for slightly better performances.

Conclusively, CNNs are not computational-friendly models in the dual-encoder multi-modal pre-training task. CNNs require more training cost than ViTs but achieve worse result. For the computational resources limited environment, ViT-B/16 is regarded as our best choice.

## 6. Training

In contrastive self-supervised learning [6, 7], distributed large-batch training has become a standard practice, for increasing the training batch size and providing enough negative samples. In the following, we first reveal the remarkable benefits of distributed large-batch training in the multi-modal pre-training task; however, it relies on considerable computational resources (*e.g.*, training our model with 16,384 batch size needs 128 V100 GPUs). To tackle this problem, we study how to achieve comparable results with limited computational resources (*e.g.*, 8 V100 GPUs).

### 6.1. Benefits of Distributed Large-batch Training

**Gradient reversed gather.** Facilitated by fast-growing deep learning frameworks, various tasks could benefit from multi-machine distributed training systems. Regarding the practical implementation of distributed contrastive loss, gather operations are frequently used to collect negative samples across machines. In the implementation (*e.g.*, `torch.distributed.all_gather` function) of PyTorch,

gradients of gathered embeddings are detached and cannot be back-propagated to their original machines. Official codes of recent contrastive learning works also noticed this problem [2, 6, 7, 15] but no relevant discussions and comparisons are elaborated. To this end, we formulate the gradients produced by the contrastive loss, and then reveal that, in the multi-modal contrastive loss, preserving gradients of gathered embeddings would provide valuable gradients<sup>1</sup>.

As reported in Table 5, by preserving gradients of gathered embeddings, noticeable gains are achieved within expectations. Concretely, +4.9 RSUM on F30K and +12.2 RSUM on MSCOCO are contributed by the gradient reversed gather, further supporting our derivations.

**Large-batch training.** Previous works have demonstrated that self-supervised contrastive learning could significantly benefit from the large training batch size, which provides more negative examples to facilitate the model convergence [6]. To further analyze the impact of varying batch sizes on multi-modal contrastive pre-training, we scale the batch size from 1,024 to 16,384 and keep training epochs consistent. Besides, previous works empirically showed that linearly scaling the initial learning rate is necessary for large-batch training. Nevertheless, there is no necessity for our method to adjust the initial learning rate. We conjecture the reason could be the adaptive optimizer, *i.e.*, the AdamW optimizer computes adaptive learning rates for different parameters, desensitizing the selection of initial learning rates.

Regarding large batch experiments, up to 128 Nvidia V100 GPUs are used. As shown in Table 5, increasing the batch size from 1,024 to 16,384 leads to significant improvements on all evaluated metrics, indicating the vital importance of large-batch training.

### 6.2. Large-batch Training with Limited Resources

Experiments in Sec. 6.1 have demonstrated the considerable improvements from large-batch training. However, substantial computational resources are used for containing large batches. For experiments in Table 5, up to 128 V100 GPUs from 16 machines are used for training with 16,384 batch size. Thus, large-batch training could be infeasible for experimental environments where computation resources are limited, *e.g.*, a single-machine with 8 GPUs.

<sup>1</sup>Due to the page limit, formulations are attached in Appendix A.1.

	MSCOCO (5K test set)							Flickr30K (1K test set)						
	image → text			text → image				image → text			text → image			
	R@1	R@5	R@10	R@1	R@5	R@10	RSUM	R@1	R@5	R@10	R@1	R@5	R@10	RSUM
data preparation	53.0	79.8	87.6	39.6	66.2	76.5	402.8	80.1	95.7	98.4	63.7	88.2	93.1	519.2
+ gradient reserved gather	55.4	81.2	88.7	42.0	69.0	78.7	415.0	81.4	95.6	98.2	66.2	89.0	93.7	524.1
+ large batch (2,048)	56.4	81.4	88.5	42.7	69.7	79.2	418.0	81.5	95.9	98.6	68.2	89.6	93.7	527.5
+ large batch (4,096)	58.9	83.1	89.9	43.8	70.5	79.6	425.9	82.7	96.7	98.6	68.7	90.4	94.5	531.7
+ large batch (8,192)	59.0	82.4	89.5	43.7	70.2	79.5	424.4	83.1	96.8	98.7	68.5	90.1	94.6	531.8
+ large batch (16,384)	59.3	82.2	89.6	44.1	70.4	79.5	425.0	85.5	97.6	98.5	69.8	90.3	94.5	536.2

Table 5. Results of training heuristics. “data preparation” denotes the result of stacking all data preparation heuristics.

batch	DGA step	effective batch	# GPU	GPU time (hr)	MSCOCO RSUM	F30K RSUM
1,024	–	1,024	8	~430	415.0	524.1
8,192	–	8,192	64	–	424.4	531.8
16,384	–	16,384	128	–	425.0	536.2
1,024	8	8,192	8	~600	424.1	532.2
1,024	16	16,384	8	~680	425.2	535.9

Table 6. RSUM scores of decoupled gradient accumulation (DGA). For experiments with batch 1,024, only 8 V100 GPUs are used. For batch 8,192 and 16,384, 64 and 128 V100 GPUs are required.

**Gradient accumulation meets InfoNCE loss.** A common strategy to mimic large-batch training is the multi-step gradient accumulation. Concretely, a training iteration of a large batch is divided into several sub-iterations, and, in each sub-iteration, the batch size is relatively small. Gradients of multiple sub-iterations are individually calculated, accumulated and jointly back-propagated. It is a practical strategy in deep learning tasks; however, to mimic the large batch InfoNCE loss, the calculation process unavoidably involves embeddings from different training sub-iterations, which are, unfortunately, not accessible across sub-iterations. Therefore, the conventional multi-step gradient accumulation is not able to enlarge the effective batch size, considerably limiting final model performances.

**Decoupled gradient accumulation.** We propose the decoupled gradient accumulation to make large-batch contrastive learning feasible for limited resources. Concretely, we mathematically decouple the gradient of a large batch into two parts<sup>2</sup>. One part of gradient is only related to embeddings within each sub-iteration, and the other part only depends on stop-gradient embeddings of the large batch, which can be obtained by forwarding the large batch for an extra time. Consequently, we are allowed to take advantages of the large batch size by sacrificing training time. As reported in Table 6, it empirically shows that, by sacrificing extra 40%–50% training time, our gradient accumulation successfully mimics large-batch training without damaging model performances. With 8 V100 GPUs, we are not allowed to train the model with batch sizes larger than 1,024, and thus achieved performances are relatively unsatisfactory. However, our method successfully allows us to train models

<sup>2</sup>Due to the page limit, formulations are attached in Appendix A.2.

training method	encoder		GPU time (hr)	MSCOCO RSUM	F30K RSUM
	image	text			
auxiliary	ViT-B/16	BERT-B	–	402.8	519.1
	ViT-B/32	BERT-B♠	~110	381.2	493.9
baseline	ViT-B/32	BERT-B	~240	379.5	494.1

Table 7. Training time saved by the auxiliary encoder method. “♠” symbol denotes the model is frozen.

with large effective batch sizes 8,192 and 16,384, achieving comparable RSUM scores with only 8 V100 GPUs.

### 6.3. Fast Training with Auxiliary Encoders

Thus far, all heuristics for better performances are elaborated. However, for real-scenario multi-modal applications, the model efficiency and performance are equally significant for various deployment purposes. Assuming that we have trained a model with heavy encoders, we investigate how to fast obtain lightweight encoders with auxiliary heavy ones.

Since the training of a dual-encoder model is driven by the InfoNCE loss, embeddings yielded by either encoder are regarded as the “learning target” of the other side. Thus, enlarging either encoder’s capacity would contribute to more reliable and discriminative embeddings. Assuming that we have trained a dual-encoder model with heavy encoders, *e.g.*, ViT-B/16 and BERT-Base, we can replace one of them to a lightweight one and re-train it with the guidance of the other one. For instance, we change the image encoder from ViT-B/16 to ViT-B/32, and then re-train it with the BERT-Base being frozen. With the guidance of the frozen encoder, the training process of the replaced encoder could be greatly accelerated. As reported in Table 7, we halve the training epoch for training the ViT-B/32, and the GPU time is greatly decreased, without damaging final results.

## 7. Comparisons with SOTA Methods

In this section, we focus on assessing the pre-training performances with cross-modal retrieval tasks, in both zero-shot and fine-tuned settings [23,38]. We name our method as “ZeroVL”, where “Zero” means the motivation for designing a strong baseline with limited resources.

	computation		data	input size	MSCOCO (5K test set)						Flickr30K (1K test set)							
	device	count			image → text			text → image			image → text			text → image				
<i>zero-shot</i>					R@1	R@5	R@10	R@1	R@5	R@10	RSUM	R@1	R@5	R@10	R@1	R@5	R@10	RSUM
CLIP	V100	256	400M	336	58.4	81.5	88.1	37.8	62.4	72.2	400.2	88.0	98.7	99.4	68.7	90.6	95.2	540.6
ALIGN	TPUv3	1,024	1800M	289	58.6	83.0	89.7	45.6	69.8	78.6	425.3	<b>88.6</b>	<b>98.7</b>	<b>99.7</b>	<b>75.7</b>	<b>93.8</b>	<b>96.8</b>	<b>553.3</b>
baseline	V100	8	14M	224	45.1	71.5	81.6	33.9	60.3	71.1	363.5	66.0	88.9	94.1	56.2	82.4	89.2	476.8
ZeroVL (ours)	V100	8	14M	224	59.3	82.2	89.6	44.1	70.4	79.5	425.0	85.5	97.6	98.5	69.8	90.3	94.5	536.2
ZeroVL† (ours)	V100	8	100M	224	<b>64.0</b>	<b>85.8</b>	<b>91.4</b>	<b>47.3</b>	<b>72.5</b>	<b>81.1</b>	<b>442.1</b>	88.0	97.9	99.2	73.5	92.2	95.7	546.5

Table 8. *Zero-shot* cross-modal retrieval results. “baseline” is the naive baseline in Sec. 3. “†” means training with the 100M web data.

	input size	encoder		MSCOCO (5K test set)						Flickr30K (1K test set)							
		image	text	image → text			text → image			image → text			text → image				
<i>fine-tuned</i>				R@1	R@5	R@10	R@1	R@5	R@10	RSUM	R@1	R@5	R@10	R@1	R@5	R@10	RSUM
UNITER	ori	F-RCNN&BERT-L		65.7	88.6	93.8	52.9	79.9	88.0	468.9	87.3	98.0	99.2	75.6	94.1	96.8	551.0
VILLA	ori	F-RCNN&BERT-L		–	–	–	–	–	–	–	87.9	97.5	98.8	76.3	94.2	96.8	551.5
OSCAR	ori	F-RCNN&BERT-L		73.5	92.2	96.0	57.5	82.8	89.8	491.8	–	–	–	–	–	–	–
GPO	512	RX101* BERT-B		68.1	90.2	95.2	52.7	80.2	88.3	474.8	88.7	98.9	99.8	76.1	94.5	97.1	555.1
ALIGN	289	Eff-L2 BERT-L		77.0	<b>93.5</b>	96.9	<b>59.9</b>	83.3	89.8	500.4	<b>95.3</b>	<b>99.8</b>	<b>100.0</b>	<b>84.9</b>	<b>97.4</b>	<b>98.6</b>	<b>576.0</b>
baseline	224	ViT-B/16 BERT-B		69.1	90.0	94.8	51.9	78.7	86.8	471.1	90.1	98.5	99.1	75.1	93.6	96.6	553.0
ZeroVL (ours)	224	ViT-B/16 BERT-B		72.9	91.5	95.9	55.1	81.0	88.6	485.0	91.7	99.0	99.5	79.2	95.1	97.1	561.6
ZeroVL† (ours)	288	ViT-B/16 BERT-B		<b>77.2</b>	93.3	<b>97.1</b>	59.3	<b>83.4</b>	<b>90.2</b>	<b>500.5</b>	95.0	99.6	100.0	83.7	96.7	98.6	573.6

Table 9. *Fine-tuned* cross-modal retrieval results. “UNITER”, “VILLA”, and “OSCAR” are single-encoder methods, which depend on Faster-RCNN (F-RCNN) [39] to extract image region features and BERT-Large to jointly embed image and text features. “RX101\*” correspond to the ResNeXt-101 model pre-trained on Instagram-1B [51]. “†” denotes pre-training with the 100M web data.

## 7.1. Zero-Shot Cross-Modal Retrieval

**Setup.** Training implementation details are as followed. On the ground of baseline settings (*e.g.*, learning rate, training epoch, and weight decay) introduced in Sec. 3.2, we stack all aforementioned heuristics, *i.e.*, debaised sampling, AutoAugment, coin flipping mixup, gradient reserved gather and decoupled gradient accumulation. For reproducibility, we mainly benchmark with publicly accessible academic datasets. Besides, CLIP and ALIGN respectively collect 400M and 1.8B image-text pairs from the web. Due to training datasets of CLIP and ALIGN are not available, we also collect  $\sim$ 100M web image-text pairs for validating the effectiveness of our method on large-scale data.

**Main results.** In Table 8, on both F30K and MSCOCO datasets, we achieve competitive results on the basis of 14M academic publicly accessible data and 8 V100 GPUs. It is worth mentioning that our ZeroVL already exceeds CLIP on the MSCOCO dataset in both image-to-text (I2T) and text-to-image (T2I) metrics, *e.g.*, our I2T R@1 and T2I R@1 surpass CLIP by +0.9 and +6.3, respectively. In addition, although our collected 100M web images are much less than those of CLIP and ALIGN, ZeroVL still successfully outperforms CLIP trained with 400M data and ALIGN trained with 1.8B data on MSCOCO. On F30K, we perform slightly worse than ALIGN but better than CLIP, which can result from the domain of ALIGN’s data is larger than ours.

**Resources costs.** For computational resources, training CLIP requires 256 V100 GPUs, and training ALIGN needs 1,024 Cloud TPUv3 cores. Experiments in Table 8 involve 8 V100 32GB GPUs. For data resources, we mainly bench-

mark on 14M publicly accessible academic datasets to guarantee the reproducibility. Experiments of 100M web data demonstrate that our method is still effective on large-scale data, *i.e.*, our method is feasible for different data scales.

## 7.2. Fine-Tuned Cross-Modal Retrieval

**Setup.** After the pre-training phase, we fine-tune the model on downstream datasets F30K and MSCOCO. Fine-tuning hyper-parameters are identical to pre-training’s, except the initial learning rate, training epoch, and batch size. The learning rate is set to  $1e-5$ . For F30K and MSCOCO, we optimize the model for 1K and 5K steps. Batch size is set to 2,048. Similar to zero-shot experiments, we also provide fine-tuning results with both 14M and 100M data.

**Main results.** In Table 9, with 14M academic pre-training data, we successfully outperforms state-of-the-art in-domain training method GPO [5] and representative single-encoder methods UNITER [8] and VILLA [14]. It is worth mentioning that GPO also involves large-scale pre-training on the image modal, *i.e.*, weakly supervised pre-training with the Instagram-1B dataset [51]. Compared with GPO, ZeroVL can achieve better results with the more efficient image encoder and smaller training input size, strongly supporting the effectiveness of our pre-training method. For experiments with 100M web data, it is worth noting that ALIGN uses (1) significantly more pre-training data, (2) heavier image and text encoders, and (3) larger pre-training resolutions than our method. Nevertheless, similar to results in zero-shot setting, our method still achieves comparable results to ALIGN.

## 8. Conclusion

This work provides a training guideline for conducting dual-encoder multi-modal representation alignment with limited resources. With only 14M publicly accessible academic datasets and 8 V100 GPUs, we provide a reproducible strong baseline. In addition, we achieve comparable or superior performances than state-of-the-art methods with 100M web data. We hope our training pipeline and benchmark will be useful for future researches in the multi-modal field.

## A. Appendix

In Sec. A.1, we discuss the gradient of multi-modal contrastive loss. In Sec. A.2, we elaborate the derivations and implementations of decoupled gradient accumulation. In Sec. A.3, we introduce the detailed calculation of coin flipping mixup loss. In Sec. A.4, we detail open-source and web pre-training data. In Sec. A.5, we provide training details for reproducing our strong baseline.

### A.1. Gradient of Multi-Modal Contrastive Loss

**Formulating gradients of contrastive loss.** Within each training batch, define the similarity between the *query*  $j$  and the *key*  $k$  as  $s_{jk}$ , which ranges from 0 to 1. The ground-truth label corresponding to  $s_{jk}$  is represented by  $y_{jk} \in \{0, 1\}$ . The contrastive loss can be formulated as:

$$\mathcal{L} = \sum_j \sum_k y_{jk} \log \left( \frac{\exp(s_{jk})}{\sum_l \exp(s_{jl})} \right), \quad (4)$$

where the temperature parameter is omitted for simplification. Then, the gradient of the popular contrastive loss could be written as:

$$\begin{aligned} \nabla_{\theta} \mathcal{L} &= - \sum_j \sum_k y_{jk} \nabla_{\theta} \log \left( \frac{\exp(s_{jk})}{\sum_l \exp(s_{jl})} \right) \\ &= - \sum_j \sum_k y_{jk} \left( \nabla_{\theta} s_{jk} - \nabla_{\theta} \log \sum_l \exp(s_{jl}) \right) \\ &= - \sum_j \sum_k y_{jk} \left( \nabla_{\theta} s_{jk} - \frac{1}{\sum_l \exp(s_{jl})} \nabla_{\theta} \sum_l \exp(s_{jl}) \right) \\ &= - \sum_j \sum_k y_{jk} \left( \nabla_{\theta} s_{jk} - \sum_l \frac{\exp(s_{jl})}{\sum_m \exp(s_{jm})} \nabla_{\theta} s_{jl} \right) \\ &= - \sum_j \sum_k y_{jk} \left( \nabla_{\theta} s_{jk} - \sum_l \bar{p}_{jl} \nabla_{\theta} s_{jl} \right) \\ &= - \sum_j \sum_k y_{jk} \nabla_{\theta} s_{jk} + \sum_j \sum_k y_{jk} \sum_l \bar{p}_{jl} \nabla_{\theta} s_{jl}, \end{aligned} \quad (5)$$

where we place a vinculum on a value to indicate its gradient is detached. Due to  $\sum_k y_{jk} = 1$ , we rewrite Eqn.(5) as:

$$\begin{aligned} \nabla_{\theta} \mathcal{L} &= - \sum_j \sum_k y_{jk} \nabla_{\theta} s_{jk} + \sum_j \sum_l \bar{p}_{jl} \nabla_{\theta} s_{jl} \\ &= - \sum_j \sum_k y_{jk} \nabla_{\theta} s_{jk} + \sum_j \sum_k \bar{p}_{jk} \nabla_{\theta} s_{jk} \\ &= \sum_j \sum_k (\bar{p}_{jk} - y_{jk}) \nabla_{\theta} s_{jk} \\ &= \sum_j \sum_k (\bar{p}_{jk} - y_{jk}) (\bar{x}_j \nabla_{\theta} x_k + \bar{x}_k \nabla_{\theta} x_j), \end{aligned} \quad (6)$$

where  $x_j$  and  $x_k$  are embeddings of sample  $j$  and  $k$ . Regarding the sample  $j$  as the *query*, its gradient comes to  $\sum_k (\bar{p}_{jk} - y_{jk}) (\bar{x}_j \nabla_{\theta} x_k + \bar{x}_k \nabla_{\theta} x_j)$ . If sample  $j$  and  $k$  are from different machines, detaching gradients makes the term  $\bar{x}_j \nabla_{\theta} x_k$  to 0, since  $x_k$  serves as a constant term in the gradient calculation process.

**Detaching gradients in multi-modal contrastive loss.** Subsequently, we study the gradients of multi-modal contrastive loss. We start with minor notation adjustments to cater for the multi-modal setting. The calculation of multi-modal contrastive loss can be divided into image-to-text (I2T) matching and text-to-image (T2I) matching parts. Gradients of I2T and T2I matching losses are:

$$\nabla_{\theta} \mathcal{L}^{I2T} = \sum_j \sum_k (\bar{p}_{jk}^{I2T} - y_{jk}^{I2T}) (\bar{i}_j \nabla_{\theta} t_k + \bar{t}_k \nabla_{\theta} i_j), \quad (7)$$

$$\nabla_{\theta} \mathcal{L}^{T2I} = \sum_j \sum_k (\bar{p}_{kj}^{T2I} - y_{kj}^{T2I}) (\bar{t}_j \nabla_{\theta} i_k + \bar{i}_k \nabla_{\theta} t_j), \quad (8)$$

where  $i$  and  $t$  represent image and text embeddings. For pairs  $(i_j, t_k)$  and  $(t_j, i_k)$  from *different* machines, gather operations with detaching gradients would produce the following gradients on the machine of  $j$ :

$$\tilde{\nabla}_{\theta} \mathcal{L}^{I2T} = \sum_j \sum_k (\bar{p}_{jk}^{I2T} - y_{jk}^{I2T}) \bar{t}_k \nabla_{\theta} i_j, \quad (9)$$

and the gradient on  $k$ 's machine:

$$\tilde{\nabla}_{\theta} \mathcal{L}^{T2I} = \sum_j \sum_k (\bar{p}_{kj}^{T2I} - y_{kj}^{T2I}) \bar{i}_j \nabla_{\theta} t_k. \quad (10)$$

We add a tilde symbol on the gradient  $\tilde{\nabla}_{\theta} \mathcal{L}$ , indicating the calculation involves detaching gradients. Then, we have:

$$\nabla_{\theta} \mathcal{L}^{I2T} + \nabla_{\theta} \mathcal{L}^{T2I} \neq (\tilde{\nabla}_{\theta} \mathcal{L}^{I2T} + \tilde{\nabla}_{\theta} \mathcal{L}^{T2I}). \quad (11)$$

Mathematically, detaching gradients in multi-modal contrastive loss yields incorrect gradients. Experiments in Sec. 6.1 of the manuscript prove that gradient reserved gather operations are beneficial in multi-modal contrastive learning.

## A.2. Decoupled Gradient Accumulation

### Decoupling the gradient of multi-modal contrastive loss.

Inspired by a blog post<sup>3</sup> which decouples the gradient of single-modal contrastive loss, we further generalize it to the multi-modal scenario. According to Eqn.(7) and (8), we have:

$$\begin{aligned}\nabla_{\theta}\mathcal{L}^{I2T} &= \sum_j \sum_k \left( \bar{p}_{jk}^{I2T} - y_{jk}^{I2T} \right) (\bar{i}_j \nabla_{\theta} t_k + \bar{t}_k \nabla_{\theta} i_j) \\ &= \sum_k \nabla_{\theta} \left( \sum_j \left( \bar{p}_{jk}^{I2T} - y_{jk}^{I2T} \right) \bar{i}_j \right) t_k \\ &\quad + \sum_j \nabla_{\theta} \left( \sum_k \left( \bar{p}_{jk}^{I2T} - y_{jk}^{I2T} \right) \bar{t}_k \right) i_j\end{aligned}\quad (12)$$

$$\begin{aligned}\nabla_{\theta}\mathcal{L}^{T2I} &= \sum_j \sum_k \left( \bar{p}_{jk}^{T2I} - y_{jk}^{T2I} \right) (\bar{t}_j \nabla_{\theta} i_k + \bar{i}_k \nabla_{\theta} t_j) \\ &= \sum_k \nabla_{\theta} \left( \sum_j \left( \bar{p}_{jk}^{T2I} - y_{jk}^{T2I} \right) \bar{t}_j \right) i_k \\ &\quad + \sum_j \nabla_{\theta} \left( \sum_k \left( \bar{p}_{jk}^{T2I} - y_{jk}^{T2I} \right) \bar{i}_k \right) t_j \\ &= \sum_j \nabla_{\theta} \left( \sum_k \left( \bar{p}_{kj}^{T2I} - y_{kj}^{T2I} \right) \bar{t}_k \right) i_j \\ &\quad + \sum_k \nabla_{\theta} \left( \sum_j \left( \bar{p}_{kj}^{T2I} - y_{kj}^{T2I} \right) \bar{i}_j \right) t_k.\end{aligned}\quad (13)$$

Then, the total gradient can be written as:

$$\begin{aligned}\nabla_{\theta}\mathcal{L} &= \nabla_{\theta}\mathcal{L}^{I2T} + \nabla_{\theta}\mathcal{L}^{T2I} \\ &= \sum_j \nabla_{\theta} \left( \sum_k \left( \bar{p}_{jk}^{I2T} - y_{jk}^{I2T} + \bar{p}_{kj}^{T2I} - y_{kj}^{T2I} \right) \bar{t}_k \right) i_j \\ &\quad + \sum_k \nabla_{\theta} \left( \sum_j \left( \bar{p}_{jk}^{I2T} - y_{jk}^{I2T} + \bar{p}_{kj}^{T2I} - y_{kj}^{T2I} \right) \bar{i}_j \right) t_k.\end{aligned}\quad (14)$$

As suggested in Eqn.(14), we mathematically decouple the gradient into two parts. One part of gradient is only related to stop-gradient embeddings ( $\bar{t}_k$  and  $\bar{i}_j$ ), and the other part only depends on embeddings with gradients ( $t_k$  and  $i_j$ ).

### Implementation of decoupled gradient accumulation.

As mentioned in the Sec. 6.2 of the manuscript, in the conventional multi-step gradient accumulation, we are not allowed to obtain embeddings (with gradients) from different training sub-iterations. However, we can cache stop-gradient embeddings of the large batch, and then calculate the correct gradient with Eqn.(14) in each sub-iteration. With forwarding the large batch and caching stop-gradient embeddings, our decoupled gradient accumulation can accurately produce the gradient produced by large-batch training.

<sup>3</sup><https://spaces.ac.cn/archives/8471>

**Stable decoupled gradient accumulation.** Note that encoders could contain modules of randomness, *e.g.*, dropout layers are widely applied in the BERT [11]. Thus, forwarding the same sample two times could produce different embeddings. To this end, we set the identical random seed for twice forwarding processes. In the following table, we provide an ablation study related to the randomness.

batch	DGA step	effective batch	# GPU	stable	MSCOCO RSUM	F30K RSUM
1,024	16	16,384	8	✓	425.2	535.9
1,024	16	16,384	8	–	413.4	527.1

“✓” denotes setting the identical random seed for twice forwarding processes, and the achieved results correspond to Table 6 of the manuscript. However, the above results demonstrate that significant performance drops would be caused without considering the randomness, *i.e.*, forwarding the same sample for two times yields different embeddings and thus gradient in Eqn.(14) is wrongly calculated. Besides, the BatchNorm (BN) layer is widely used in convolutional networks but can cause inconsistent statistics between the sub-batches and the large batch, resulting in wrong gradients. However, our method uses Transformer-based encoders and only LayerNorm (LN) layers are used, and the calculation of statistics is not relevant to batch size. It further demonstrates the superiority of Transformer-based encoders.

**Pseudo code in a PyTorch-like style.** As shown in Algorithm 1, we provide a pseudo code of decoupled gradient accumulation for better understanding. In the implementation of previous methods [23, 38], the temperature of contrastive loss is learnable. Thus, in the implementation of decoupled gradient accumulation, we need consider the gradient of the temperature variable. As shown in Algorithm 1, we detach the gradient of temperature (with `torch.no_grad`) for forwarding the large batch, and then calculate the gradient of temperature in each sub-iteration. Besides, a square-root should be applied on the value of temperature for correctly calculating the scale of temperature.

## A.3. Coin Flipping Mixup Loss

We detail the coin flipping mixup loss function by following notations defined in Sec. 4.2 of the manuscript. We first define a batch  $\{(I_1, T_1), (I_2, T_2), \dots, (I_N, T_N)\}$  of  $N$  image-text pairs. Then, we uniformly sample a  $\gamma$  from the range  $[0, 1]$ .

$\gamma > 0.5$ : We apply the mixup on the images, and the mixed batch can be denoted as  $\{(\tilde{I}_1, T_1), (\tilde{I}_2, T_2), \dots, (\tilde{I}_N, T_N)\}$ .

---

**Algorithm 1** Pseudo code in a PyTorch-like style.

---

```
# stable_random_seed: random seed generated by time.time()
# temp: temperature

# fix dropout with fixed random seed
setup_seed(random_seed)

with torch.no_grad():
    # stop-grad forward
    img_emb_local, text_emb_local = [], []
    for _idx_l in range(0, bs, bs_train):
        _data_batch = data_batch[_idx_l: _idx_l + bs_train]
        _img_embs, _text_embs, temp = model(_data_batch)
        img_emb_local.append(_img_embs)
        text_emb_local.append(_text_embs)

    # concatenate embeddings of each GPU
    img_emb_local = torch.cat(img_emb_local, dim = 0)
    text_emb_local = torch.cat(text_emb_local, dim = 0)

    # gather embeddings of all GPUs
    img_emb_global = torch.cat(gather(img_emb_local), dim = 0)
    text_emb_global = torch.cat(gather(text_emb_local), dim = 0)

    # calculate cosine similarity
    sim_i2t_nm = img_emb_global @ text_emb_local.T / temp
    sim_i2t_mn = img_emb_local @ text_emb_global.T / temp

    # calculate the normalized factor in softmax function
    sim_i2t_esum_local = torch.sum(torch.exp(sim_i2t_mn), dim = 1)
    sim_t2i_esum_local = torch.sum(torch.exp(sim_i2t_nm.T), dim = 1)
    sim_i2t_esum = torch.cat(gather(sim_i2t_esum_local), 0).unsqueeze(dim = 1)
    sim_t2i_esum = torch.cat(gather(sim_t2i_esum_local), 0).unsqueeze(dim = 1)

    # calculate the probability matrix
    prob_i2t_nm = torch.exp(sim_i2t_nm) / sim_i2t_esum[bs * rank: bs * (rank + 1), :]
    prob_t2i_nm = torch.exp(sim_i2t_nm.T) / sim_t2i_esum
    prob_i2t_mn = torch.exp(sim_i2t_mn) / sim_i2t_esum
    prob_t2i_mn = torch.exp(sim_i2t_mn.T) / sim_t2i_esum[bs * rank: bs * (rank + 1), :]

    left_I = (prob_i2t_mn + prob_t2i_nm.T) @ text_emb_global - text_emb_local * 2 / torch.sqrt(temp)
    left_T = (prob_i2t_nm.T + prob_t2i_mn) @ img_emb_global - img_emb_local * 2 / torch.sqrt(temp)

# Fix dropout with fixed random seed
setup_seed(random_seed)

# forward with grad
for _idx_l in range(0, bs, bs_train):
    _left_I = left_I[_idx_l: _idx_l + bs_train]
    _left_T = left_T[_idx_l: _idx_l + bs_train]
    _data_batch = data_batch[_idx_l: _idx_l + bs_train]

    _img_embs, _text_embs, temp = model(_data_batch)

    loss_i = _left_I * _img_embs
    loss_t = _left_T * _text_embs
    # loss corresponds to Eqn.(14)
    loss = (loss_i + loss_t).sum() / 2 / bs / torch.sqrt(temp)
    # backward propagation
    loss.backward()

# update model parameters
update(model.param)
```

---

The image-to-text matching part can be formulated as:

$$\begin{aligned} \mathcal{L}_{\tilde{I}2T} = & \lambda * \left( -\frac{1}{N} \sum_{j=1}^N \log \frac{\exp(\tilde{i}_j \cdot t_j / \tau)}{\sum_{k=1}^N \exp(\tilde{i}_j \cdot t_k / \tau)} \right) \\ & + (1 - \lambda) * \left( -\frac{1}{N} \sum_{j=1}^N \log \frac{\exp(\tilde{i}_j \cdot t_{N-j} / \tau)}{\sum_{k=0}^{N-1} \exp(\tilde{i}_j \cdot t_{N-k} / \tau)} \right). \end{aligned} \quad (15)$$

And the text-to-image part can be formulated as:

$$\begin{aligned} \mathcal{L}_{T2\tilde{I}} = & \lambda * \left( -\frac{1}{N} \sum_{j=1}^N \log \frac{\exp(t_j \cdot \tilde{i}_j / \tau)}{\sum_{k=1}^N \exp(t_j \cdot \tilde{i}_k / \tau)} \right) \\ & + (1 - \lambda) * \left( -\frac{1}{N} \sum_{j=1}^N \log \frac{\exp(t_j \cdot \tilde{i}_{N-j} / \tau)}{\sum_{k=0}^{N-1} \exp(t_j \cdot \tilde{i}_{N-k} / \tau)} \right). \end{aligned} \quad (16)$$

$\gamma \leq 0.5$ : We apply the mixup on the texts, and the mixed batch can be denoted as  $\{(I_1, \tilde{T}_1), (I_2, \tilde{T}_2), \dots, (I_N, \tilde{T}_N)\}$ . The image-to-text matching part can be formulated as:

$$\begin{aligned} \mathcal{L}_{I2\tilde{T}} = & \lambda * \left( -\frac{1}{N} \sum_{j=1}^N \log \frac{\exp(i_j \cdot \tilde{t}_j / \tau)}{\sum_{k=1}^N \exp(i_j \cdot \tilde{t}_k / \tau)} \right) \\ & + (1 - \lambda) * \left( -\frac{1}{N} \sum_{j=1}^N \log \frac{\exp(i_j \cdot \tilde{t}_{N-j} / \tau)}{\sum_{k=0}^{N-1} \exp(i_j \cdot \tilde{t}_{N-k} / \tau)} \right). \end{aligned} \quad (17)$$

And the text-to-image part can be formulated as:

$$\begin{aligned} \mathcal{L}_{\tilde{T}2I} = & \lambda * \left( -\frac{1}{N} \sum_{j=1}^N \log \frac{\exp(\tilde{t}_j \cdot i_j / \tau)}{\sum_{k=1}^N \exp(\tilde{t}_j \cdot i_k / \tau)} \right) \\ & + (1 - \lambda) * \left( -\frac{1}{N} \sum_{j=1}^N \log \frac{\exp(\tilde{t}_j \cdot i_{N-j} / \tau)}{\sum_{k=0}^{N-1} \exp(\tilde{t}_j \cdot i_{N-k} / \tau)} \right). \end{aligned} \quad (18)$$

Generally, the coin flipping mixup loss  $\mathcal{L}_{\text{coin}}$  can be formulated as:

$$\mathcal{L}_{\text{coin}} = \begin{cases} \mathcal{L}_{\tilde{I}2T} + \mathcal{L}_{T2\tilde{I}}, & \text{if } \gamma > 0.5 \\ \mathcal{L}_{I2\tilde{T}} + \mathcal{L}_{\tilde{T}2I}, & \text{if } \gamma \leq 0.5. \end{cases} \quad (19)$$

#### A.4. Details of Pre-Training Datasets

**Open-source datasets.** Four widely-used image-text pair datasets are selected for pre-training. Details are as followed:

- SBU Captioned Photos (SBU) [36] contains 1M images with associated visually relevant captions.
- Visual Genome (VG) [28] consists of around 100K images and 5M captions, where each image is coupled with 50 captions. For training efficiency, we filter 5 out of 50 captions for each image according to largest areas of bounding box regions.
- Conceptual Captions 3M (CC3M) [40] contains around 3.3M images annotated with captions, collected from web data with an automatic collection pipeline.

- Conceptual 12M (CC12M) [3] is similar to CC3M and the collection pipeline is relaxed. Consequently, the data in CC12M is relatively noisier than CC3M.

A part of download links provided by CC3M and CC12M are lost. Collectively, our visual-linguistic corpus for pre-training is composed of around 14.23M image-text pairs from various domains.

**Web data.** The web data is mainly collected from the Tuchong image library community<sup>4</sup>. Each image is coupled with a caption created by the image’s author. We collect around 100M image-text pairs for pre-training.

#### A.5. Training Details

We elaborate the training details of our strong baseline.

**Data preparation.** Batches are comprised by applying the debaised sampling strategy on academic pre-training datasets, *i.e.*, SBU, VG, CC3M and CC12M. Each image is randomly cropped to a rectangular region with aspect ratio sampled in  $[3/4, 4/3]$  and area sampled in  $[60\%, 100\%]$ , then resized to  $224 \times 224$  resolution. Regarding the corresponding text, we set the max length to 25 and use a percentage of 20% input words for processing. For each word, we mask it, replace it with a random word, or delete it with a probability of 50%, 10% and 40%, respectively. We directly apply AutoAugment after crop operation and the policy is search on ImageNet<sup>5</sup>. Coin flipping mixup is also used in the training phase, and the  $\alpha$  is set to 0.1 in the coin flipping mixup. During test, images are resized to  $256 \times 256$  and center cropped to  $224 \times 224$ , while no specific process is applied to texts.

**Model architecture.** Image and text encoders are ViT-B/16 and BERT-Base, respectively. The image encoder is pre-trained on ImageNet-21K from the timm<sup>6</sup> library while the text encoder is pre-trained on BookCorpus and English Wikipedia from the HuggingFace<sup>7</sup> library. [CLS] tokens from image and text encoders are extracted and then projected to 512-dim compact embeddings and  $\ell_2$  normalized for calculating the contrastive loss.

**Training.** AdamW optimizer is used for training and the weight decay is  $1e-3$ . Based on our decoupled gradient accumulation, the dual-encoder model is trained for 20 epochs on 8 Nvidia V100 GPUs with a batch size of 16,384. The learning rate is initialized to  $1e-4$  and follows a cosine decay schedule. Notably, we set a minimum learning rate  $1e-5$  to avoid over-fitting. The embedding dimension for image and text representations is 512 and the trainable temperature of contrastive loss is initialized to 0.02.

<sup>4</sup><https://www.tuchong.com>

<sup>5</sup><https://github.com/4uiiurz1/pytorch-auto-augment>

<sup>6</sup><https://github.com/rwightman/pytorch-image-models>

<sup>7</sup><https://huggingface.co>

## References

- [1] Stanislaw Antol, Aishwarya Agrawal, Jiaseen Lu, Margaret Mitchell, Dhruv Batra, C. Lawrence Zitnick, and Devi Parikh. VQA: Visual Question Answering. In *ICCV*, 2015. 1
- [2] Mathilde Caron, Hugo Touvron, Ishan Misra, Hervé Jégou, Julien Mairal, Piotr Bojanowski, and Armand Joulin. Emerging properties in self-supervised vision transformers. *arXiv:2104.14294*, 2021. 6
- [3] Soravit Changpinyo, Piyush Sharma, Nan Ding, and Radu Soricut. Conceptual 12M: Pushing web-scale image-text pre-training to recognize long-tail visual concepts. In *CVPR*, 2021. 2, 12
- [4] Hui Chen, Guiguang Ding, Xudong Liu, Zijia Lin, Ji Liu, and Jungong Han. Imram: Iterative matching with recurrent attention memory for cross-modal image-text retrieval. In *CVPR*, 2020. 1, 3
- [5] Jiacheng Chen, Hexiang Hu, Hao Wu, Yuning Jiang, and Changhu Wang. Learning the best pooling strategy for visual semantic embedding. In *CVPR*, 2021. 1, 2, 3, 8
- [6] Ting Chen, Simon Kornblith, Mohammad Norouzi, and Geoffrey Hinton. A simple framework for contrastive learning of visual representations. In *ICML*, 2020. 1, 6
- [7] Ting Chen, Simon Kornblith, Kevin Swersky, Mohammad Norouzi, and Geoffrey Hinton. Big self-supervised models are strong semi-supervised learners. In *NeurIPS*, 2020. 1, 6
- [8] Yen-Chun Chen, Linjie Li, Licheng Yu, Ahmed El Kholy, Faisal Ahmed, Zhe Gan, Yu Cheng, and Jingjing Liu. UNITER: Universal image-text representation learning. In *ECCV*, 2020. 1, 2, 8
- [9] Ekin D Cubuk, Barret Zoph, Dandelion Mane, Vijay Vasudevan, and Quoc V Le. AutoAugment: Learning augmentation strategies from data. In *CVPR*, 2019. 4
- [10] Jia Deng, Wei Dong, Richard Socher, Li-Jia Li, Kai Li, and Li Fei-Fei. Imagenet: A large-scale hierarchical image database. In *CVPR*, 2009. 2, 4
- [11] Jacob Devlin, Ming-Wei Chang, Kenton Lee, and Kristina Toutanova. BERT: Pre-training of deep bidirectional transformers for language understanding. *arXiv:1810.04805*, 2018. 1, 2, 5, 10
- [12] Alexey Dosovitskiy, Lucas Beyer, Alexander Kolesnikov, Dirk Weissenborn, Xiaohua Zhai, Thomas Unterthiner, Mostafa Dehghani, Matthias Minderer, Georg Heigold, Sylvain Gelly, et al. An image is worth 16x16 words: Transformers for image recognition at scale. In *ICLR*, 2021. 2, 5, 6
- [13] Fartash Faghri, David J Fleet, Jamie Ryan Kiros, and Sanja Fidler. VSE++: Improving visual-semantic embeddings with hard negatives. In *BMVC*, 2018. 3
- [14] Zhe Gan, Yen-Chun Chen, Linjie Li, Chen Zhu, Yu Cheng, and Jingjing Liu. Large-scale adversarial training for vision-and-language representation learning. In *NeurIPS*, 2020. 1, 2, 8
- [15] Priya Goyal, Quentin Duval, Jeremy Reizenstein, Matthew Leavitt, Min Xu, Benjamin Lefaudeux, Mannat Singh, Vinicius Reis, Mathilde Caron, Piotr Bojanowski, Armand Joulin, and Ishan Misra. VISSL. <https://github.com/facebookresearch/vissl>, 2021. 6
- [16] Yash Goyal, Tejas Khot, Douglas Summers-Stay, Dhruv Batra, and Devi Parikh. Making the V in VQA matter: Elevating the role of image understanding in Visual Question Answering. In *CVPR*, 2017. 1
- [17] Hongyu Guo, Yongyi Mao, and Richong Zhang. Augmenting data with mixup for sentence classification: An empirical study. *arXiv:1905.08941*, 2019. 4
- [18] Kaiming He, Haoqi Fan, Yuxin Wu, Saining Xie, and Ross Girshick. Momentum contrast for unsupervised visual representation learning. In *CVPR*, 2020. 1
- [19] Kaiming He, Xiangyu Zhang, Shaoqing Ren, and Jian Sun. Deep residual learning for image recognition. In *CVPR*, 2016. 6
- [20] Pengcheng He, Xiaodong Liu, Jianfeng Gao, and Weizhu Chen. DeBERTa: Decoding-enhanced bert with disentangled attention. In *ICLR*, 2021. 1, 5
- [21] Zhicheng Huang, Zhaoyang Zeng, Yupan Huang, Bei Liu, Dongmei Fu, and Jianlong Fu. Seeing Out of the box: End-to-end pre-training for vision-language representation learning. In *CVPR*, 2021. 1, 2
- [22] Herve Jegou, Matthijs Douze, and Cordelia Schmid. Product quantization for nearest neighbor search. *TPAMI*, 2010. 1
- [23] Chao Jia, Yinfei Yang, Ye Xia, Yi-Ting Chen, Zarana Parekh, Hieu Pham, Quoc V Le, Yunhsuan Sung, Zhen Li, and Tom Duerig. Scaling up visual and vision-language representation learning with noisy text supervision. In *ICML*, 2021. 1, 2, 3, 5, 7, 10
- [24] Wonjae Kim, Bokyoung Son, and Ildoo Kim. ViLT: Vision-and-language transformer without convolution or region supervision. In *ICML*, 2021. 1, 2
- [25] Diederik P Kingma and Jimmy Ba. Adam: A method for stochastic optimization. In *ICLR*, 2015. 3
- [26] Ryan Kiros, Yukun Zhu, Russ R Salakhutdinov, Richard Zemel, Raquel Urtasun, Antonio Torralba, and Sanja Fidler. Skip-thought vectors. In *NeurIPS*, 2015. 2
- [27] Alexander Kolesnikov, Lucas Beyer, Xiaohua Zhai, Joan Puigcerver, Jessica Yung, Sylvain Gelly, and Neil Houlsby. Big transfer (BIT): General visual representation learning. In *ECCV*, 2020. 6
- [28] Ranjay Krishna, Yuke Zhu, Oliver Groth, Justin Johnson, Kenji Hata, Joshua Kravitz, Stephanie Chen, Yannis Kalantidis, Li-Jia Li, David A Shamma, et al. Visual Genome: Connecting language and vision using crowdsourced dense image annotations. In *IJCV*, 2017. 2, 12
- [29] Junnan Li, Ramprasaath R Selvaraju, Akhilesh Deepak Gotmare, Shafiq Joty, Caiming Xiong, and Steven Hoi. Align before fuse: Vision and language representation learning with momentum distillation. In *NeurIPS*, 2021. 2
- [30] Liunian Harold Li, Mark Yatskar, Da Yin, Cho-Jui Hsieh, and Kai-Wei Chang. VisualBERT: A simple and performant baseline for vision and language. *arXiv:1908.03557*, 2019. 1, 2
- [31] Xiujun Li, Xi Yin, Chunyuan Li, Pengchuan Zhang, Xiaowei Hu, Lei Zhang, Lijuan Wang, Houdong Hu, Li Dong, Furu Wei, et al. OSACR: Object-semantics aligned pre-training for vision-language tasks. In *ECCV*, 2020. 1, 2

- [32] Yinhan Liu, Myle Ott, Naman Goyal, Jingfei Du, Mandar Joshi, Danqi Chen, Omer Levy, Mike Lewis, Luke Zettlemoyer, and Veselin Stoyanov. Roberta: A robustly optimized bert pretraining approach. *arXiv:1907.11692*, 2019. 1, 5
- [33] Ze Liu, Yutong Lin, Yue Cao, Han Hu, Yixuan Wei, Zheng Zhang, Stephen Lin, and Baining Guo. Swin transformer: Hierarchical vision transformer using shifted windows. In *ICCV*, 2021. 5, 6
- [34] Ilya Loshchilov and Frank Hutter. Decoupled weight decay regularization. In *ICLR*, 2019. 3
- [35] Jiasen Lu, Dhruv Batra, Devi Parikh, and Stefan Lee. ViL-BERT: Pretraining task-agnostic visiolinguistic representations for vision-and-language tasks. *arXiv:1908.02265*, 2019. 1, 2
- [36] Vicente Ordonez, Girish Kulkarni, and Tamara Berg. Im2text: Describing images using 1 million captioned photographs. In *NeurIPS*, 2011. 2, 12
- [37] Or Patashnik, Zongze Wu, Eli Shechtman, Daniel Cohen-Or, and Dani Lischinski. StyleCLIP: Text-driven manipulation of stylegan imagery. In *ICCV*, 2021. 1
- [38] Alec Radford, Jong Wook Kim, Chris Hallacy, Aditya Ramesh, Gabriel Goh, Sandhini Agarwal, Girish Sastry, Amanda Askell, Pamela Mishkin, Jack Clark, et al. Learning transferable visual models from natural language supervision. In *ICML*, 2021. 1, 2, 3, 5, 7, 10
- [39] Shaoqing Ren, Kaiming He, Ross Girshick, and Jian Sun. Faster R-CNN: Towards real-time object detection with region proposal networks. In *NeurIPS*, 2015. 8
- [40] Piyush Sharma, Nan Ding, Sebastian Goodman, and Radu Soricut. Conceptual Captions: A cleaned, hypernymed, image alt-text dataset for automatic image captioning. In *ACL*, 2018. 2, 12
- [41] Weijie Su, Xizhou Zhu, Yue Cao, Bin Li, Lewei Lu, Furu Wei, and Jifeng Dai. VL-BERT: Pre-training of generic visual-linguistic representations. *arXiv:1908.08530*, 2019. 1, 2
- [42] Alane Suhr, Mike Lewis, James Yeh, and Yoav Artzi. A corpus of natural language for visual reasoning. In *ACL*, 2017. 1
- [43] Alane Suhr, Stephanie Zhou, Ally Zhang, Iris Zhang, Huajun Bai, and Yoav Artzi. A corpus for reasoning about natural language grounded in photographs. In *ACL*, 2019. 1
- [44] Chen Sun, Austin Myers, Carl Vondrick, Kevin Murphy, and Cordelia Schmid. VideoBERT: A joint model for video and language representation learning. In *ICCV*, 2019. 1, 2
- [45] Hao Tan and Mohit Bansal. LXMERT: Learning cross-modality encoder representations from transformers. In *EMNLP*, 2019. 1, 2
- [46] Mingxing Tan and Quoc Le. Efficientnet: Rethinking model scaling for convolutional neural networks. In *ICML*, 2019. 5
- [47] Mingxing Tan and Quoc V Le. EfficientnetV2: Smaller models and faster training. In *ICML*, 2021. 6
- [48] Vikas Verma, Alex Lamb, Christopher Beckham, Amir Najafi, Ioannis Mitliagkas, David Lopez-Paz, and Yoshua Bengio. Manifold mixup: Better representations by interpolating hidden states. In *ICML*, 2019. 4
- [49] Hao Wu, Jiayuan Mao, Yufeng Zhang, Yuning Jiang, Lei Li, Weiwei Sun, and Wei-Ying Ma. Unified visual-semantic embeddings: Bridging vision and language with structured meaning representations. In *CVPR*, 2019. 1, 3
- [50] Qizhe Xie, Minh-Thang Luong, Eduard Hovy, and Quoc V Le. Self-training with noisy student improves imagenet classification. In *CVPR*, 2020. 5
- [51] I Zeki Yalniz, Hervé Jégou, Kan Chen, Manohar Paluri, and Dhruv Mahajan. Billion-scale semi-supervised learning for image classification. *arXiv:1905.00546*, 2019. 1, 8
- [52] Sangdoon Yun, Dongyoon Han, Seong Joon Oh, Sanghyuk Chun, Junsuk Choe, and Youngjoon Yoo. CutMix: Regularization strategy to train strong classifiers with localizable features. In *ICCV*, 2019. 4
- [53] Rowan Zellers, Yonatan Bisk, Ali Farhadi, and Yejin Choi. From recognition to cognition: Visual commonsense reasoning. In *CVPR*, 2019. 1
- [54] Hongyi Zhang, Moustapha Cisse, Yann N Dauphin, and David Lopez-Paz. Mixup: Beyond empirical risk minimization. In *ICLR*, 2018. 4
- [55] Peng Zhang, Yash Goyal, Douglas Summers-Stay, Dhruv Batra, and Devi Parikh. Yin and Yang: Balancing and answering binary visual questions. In *CVPR*, 2016. 1
- [56] Pengchuan Zhang, Xiujun Li, Xiaowei Hu, Jianwei Yang, Lei Zhang, Lijuan Wang, Yejin Choi, and Jianfeng Gao. VinVL: Revisiting visual representations in vision-language models. In *CVPR*, 2021. 1, 2